Improved Edge Refinement Filter with Entropy Feedback Measurement for Retrieving Region of Interest and Blind Image Deconvolution

Ahmad Husni MOHD SHAPRI[1], Mohd Zaid ABDULLAH[2]

[1]*School of Microelectronic Engineering, Universiti Malaysia Perlis,*
Pauh Putra Campus, 02600 Arau, Perlis, Malaysia
[2]*School of Electrical and Electronic Engineering, Universiti Sains Malaysia,*
Engineering Campus, 14300 Nibong Tebal, Penang, Malaysia
mza@usm.my

Abstract—**This study proposes an improved edge refinement filter with entropy feedback measurement for locating an optimal region of interest (ROI) in blurry images. This technique is inspired by He et al.'s algorithm and enhanced by introducing a suitable filter to obtain smooth unwanted pixels whilst retaining important and significant edges. This approach led to an accurate retrieval of ROI and a considerably precise image restoration within a blind deconvolution framework. Results show that the proposed method is more competitive than existing techniques and achieves better performance in terms of peak signal-to-noise ratio, kernel similarity index and error ratio.**

Index Terms—**image restoration, image edge detection, deconvolution, filtering, image enhancement.**

I. INTRODUCTION

Blind image deconvolution (BID) is a strategy used to recover or restore images that have been degraded by an unknown source of degradation or point spread function (PSF). This problem exists in many practical applications, such as the atmospheric turbulent introduced during astronomical observations, degradation resulting from out-of-focus imaging device and aliasing caused by sampling and quantisation errors. Accordingly, solving this type of image restoration problem remains a challenge owing to the ill-posed characteristic of the inversion formula, thereby often leading to unknown solutions. This problem is traditionally solved by utilising blurred images as a constraint and using this information to estimate the impulse response of a degradation system. This approach has been shown to improve the condition of BID and yield reasonably accurate solutions [1]. Nevertheless, this method requires accurate localisation of the region of interest (ROI) because not all pixels in the input image are meaningful. For example, smooth regions contain extremely limited little information, thereby failing to contribute significantly to the PSF estimation. This problem leads to several solutions, such as the use of edges as a means to retrieve an optimal and nearly optimal ROI [2–4]. Nevertheless, the edge detection of blurry or noisy images is difficult because of the loss or incomplete edge information. Pixel-based edge detection methods, such as Sobel, Prewitt, Roberts and Canny filters, have difficulties satisfying accuracy requirements owing to their low precision and high false positive. Consequently, the development of subpixel techniques for detecting edges in blurry images constitutes one of the active research areas in image processing. Some studies have been performed and interesting results have been published. Choudhary et al. [5] proposed pre-processing techniques on the basis of the Wiener filter to reduce the blurriness of images prior to detecting edges using power spectrum function. Ying et al. [6] proposed the detection method on the basis of cubic spline interpolation to improve the detection accuracy of motion-blurred images. By analysing the greyscale distribution of objects in different directions, these studies decomposed images into sub-bands, from which the noise and edge are removed and enhanced, respectively. The experimental results have suggested that the proposed method avoids the misdetection of important edges and obtains relatively high detection accuracy.

Li et al. [7] introduced a localising method for removing outlier points using the random sample consensus (RANSAC) algorithm. The experimental results have suggested that this method outperforms the standard Gaussian and Canny filters when detecting edges in blurry images. Li et al. [8] used a fuzzy prediction method to retrieve latent edges, and utilised a pyramid scheme to accelerate the search. Cho and Lee [9] used shock filter and gradient thresholding to detect noisy edges in motion-blurred images. The results from their experiments have suggested that the algorithm performs acceptably well if the edges have strong global features. However, this algorithm may converge to a local minimum in the presence of strong local features, such as isolated bright spots, thereby resulting in noisy and dense estimate. To solve this problem, relatively small patches were used instead of masks for edge denoising, such as the method proposed by Pan et al. [10]. Their algorithm performed reasonably well, particularly when the image patches have many rich details. However, if the images are lack texture or contain significantly saturated pixels, then the algorithm may behave erratically.

One solution to this problem is the research published by Hu and Yang [11]. The aforementioned study used a search technique based on a learning strategy to find small patches with elevated information content. This research formulated an algorithm based on the conditional random field framework by utilising small sub-window image structures. Although this algorithm enables the automatic selection of

good patches, the method is considerably time-consuming. Li et al. [12] provided a slightly improved approach is that published by. The aforementioned research proposed a technique based on relative total variation (RTV) to discriminate between smooth and textured regions, thereby leading to a substantially accurate PSF estimation. However, Li et al.'s algorithm relies on the accurate determination of threshold values that has to be fixed through trial-and-error. This approach is a principal drawback of the aforementioned study's algorithm. Ma et al. [13] presented a salient patch-based technique for detecting fine square regions for kernel estimation in image deblurring. This study used the structure richness and local contrast of images from which a salient patch in a refined map is determined. Experiments involving large images indicate the superiority of this algorithm in terms of sensitivity and speed compared with other blind deblurring techniques [14–15]. However, this method focuses only on uniform motion blur. Therefore, the algorithm may not function properly with other blurring artefacts, particularly when images contain smooth shades and complex sceneries. He et al. [16] proposed a guided filter in an attempt to preserve edges whilst smoothing images. The algorithm works by diffusing the background whilst relatively conserving the foreground areas similar to a bilateral filter [17]. Although this method is capable of recovering important or significant edges, small and diminutive details are lost as a result of background filtering. Another approach is to assume a certain discontinuity of edge signals and use this information to search for edges; this method is similar to the algorithm proposed by Trujillo-Pino et al. [18]. Although this method produced high precision, it is sensitive to noise and other image artefacts. Another recent approach is the method published by Jia et al. [19] based on a two-level fusion model. Although this algorithm outperforms other baseline edge detectors, the accuracy depends on the threshold scale coefficient value, which has to be set empirically. Compared with other state-of-the-art methods, He et al.'s algorithm [16] appears to presents significant improvement and technical breakthrough in the edge detection of blurry images. This algorithm is further refined in the current study to preserve as many details as possible, thereby ultimately resulting in a considerably accurate localisation of ROI. To the best of our knowledge, the present study is the first attempt in using guided filter to retrieve ROI in blurry images and blind deconvolution.

II. PROPOSED METHOD

This research introduces an improved edge refinement filter. This technique is based on an explicit guided image filter developed originally by He et al. [16]. The guided filter was derived from a local linear model and computes the filtering output by considering the content of a guidance image, which can be the input image itself or another different image. The key assumption of the guided filter is a local linear model between guidance I and filtering output q. By assuming that q is a linear transform of I in a window ω_k centred at the pixel k, then:

$$q_i = a_k I_i + b_k, \forall i \in \omega_k, \tag{1}$$

where (a_k, b_k) are linear coefficients assumed to be constant in ω_k. A square window of a radius r is used. This local linear model ensures that q has an edge if the equality $\nabla q = a \nabla I$ is fulfilled. By referring to (1), a_k and b_k should be calculated to compute q_i for a given I_i. Such a calculation requires constraints from the filtering input p such that:

$$q_i = p_i - n_i, \tag{2}$$

where n_i is the ith noisy pixel or unwanted component. Thereafter, a solution that minimises the difference between q and p whilst maintaining the linear model in (1) is determined. Specifically, the following cost function in the window ω_k is minimised:

$$E(a_k, b_k) = \sum_{i \in \omega_k} \left((a_k I_i + b_k - p_i)^2 \right) + \varepsilon a_k^2, \tag{3}$$

where ε is a regularisation parameter penalising large a_k. In this case, (3) is the linear regression model, and its solution is given by [20] as follows:

$$a_k = \frac{\frac{1}{|\omega|} \sum_{i \in \omega_k} I_i p_i - \mu_k \overline{p}_k}{\sigma_k^2 + \varepsilon} \tag{4}$$

and

$$b_k = \overline{p}_k - a_k \mu_k, \tag{5}$$

where μ_k and σ_k^2 are the mean and variance, respectively, of I in ω_k, $|\omega|$ is the number of pixels in ω_k, and $\overline{p}_k = \frac{1}{|\omega|} \sum_{i \in \omega_k} p_i$ is the mean of p in ω_k. After obtaining the linear coefficients (a_k, b_k), the filtering output q_i can be computed using (1).

One problem in the preceding calculations arises from the overlapping windows ω_k, thereby possibly resulting in a different q_i when (1) is computed in different windows. A simple strategy is to obtain the average of all the possible values of q_i. Therefore, the filtering output is calculated after computing (a_k, b_k) for all windows ω_k in the image. Mathematically:

$$q_i = \frac{1}{|\omega|} \sum_{k|i \in \omega_k} (a_k I_i + b_k). \tag{6}$$

Given that $\sum_{k|i \in \omega_k} a_k = \sum_{k \in \omega_i} a_k$ owing to the symmetry of the box window, (6) can be rewritten as follows:

$$q_i = \overline{a}_i I_i + \overline{b}_i, \tag{7}$$

where

$$\overline{a}_i = \frac{1}{|\omega|} \sum_{k \in \omega_i} a_k \tag{8}$$

and

$$\overline{b}_i = \frac{1}{|\omega|}\sum_{k\in\omega_i} b_k \qquad (9)$$

are the average coefficients of all windows overlapping i. The averaging strategy of the overlapping windows is common in image denoising, and it is a building block of the effective block-matching and 3D filtering (BM3D) algorithm [21]. However, this algorithm has one particular drawback despite effectively detecting edges. The methods and procedures tend to work less satisfactorily for low contrast images, thereby producing halos or disjointed edges in some segmented results. This problem is due to the use of local operator or guided image, which causes difficulty in determining which edge should be smoothed and preserved.

Therefore, a new edge refinement filter is proposed by modifying (7) of the original guided filter. The basic idea is to enhance the capability of the guided filter in edge detection through convolution with a suitable filter. Mathematically:

$$q_i = (\overline{a}_i + \overline{b}_i) * h_i \qquad (10)$$

where h_i is a Gaussian 2D high-pass filter and '$*$' indicates the convolution. The guided image I has been removed from (10) but remains as a parameter in calculating the average coefficient $\overline{a}_i$ as in (8).

In this case, the Gaussian 2D high-pass filter is introduced to smoothen the background, thereby increasing the overall contrast of the image, including the edges. The Gaussian 2D high-pass filter is given by [22] as follows:

$$h_i = 1 - hlp_i, \qquad (11)$$

where hlp_i is the transfer function of the corresponding 2D Gaussian low-pass filter. The general transfer function of this filter is given as follows:

$$hlp(x, y) = \frac{1}{2\pi\sigma^2} e^{-\frac{x^2 + y^2}{2\sigma^2}}, \qquad (12)$$

where the parameter σ denotes the standard deviation of the Gaussian curve, which is also related to the cut-off frequency of the filter. Equations (11) and (12) show that the transition from stop-band is extremely sharp at σ, with all frequencies above the cut-off frequency are allowed to pass through whilst attenuating other unwanted frequencies. Typically, a σ below 1 eliminates the zero-frequency component, thereby resulting in a near-black image, whereas a σ above 1 generates a sharp image. This effect is similar to high-boost filtering or unsharp masking [23]. Therefore, this parameter allows the smoothness of the Gaussian filter to be regulated.

Using (11) and (12), the method for edge recovery and image restoration is developed. A flowchart shown in Fig. 1 summarises the overall procedures. Firstly, the algorithm starts by transforming an input image to its greyscale counterpart. Secondly, the greyscale output is pre-processed using contrast limited adaptive histogram equalisation (CLAHE) [24] to increase the contrast between the foreground and background pixels. Consequently, the overall appearance of an image, including the edges, is improved. The same image is fed to the ROI search algorithm, which comprises the proposed edge refinement

filter, edge detection, morphological processing and edge partitioning. In this scenario, Canny's filter is used for edge detection, and the standard erosion and dilation techniques are applied to morphologically increase edge thickness. The outputs from this algorithm are ROI candidates based on the edge information feedback. The flowchart shows that these image processing procedures are performed in parallel. Thirdly, all ROIs retrieved from the previous step are mapped onto their corresponding locations in the enhanced image after which their entropies are calculated. ROI corresponding to the highest entropy is retrieved, and PSF is estimated thereafter. This information is used to perform image restoration using the standard BID framework. Interested readers are referred to papers published elsewhere on algorithms used for PSF estimation BID restoration [25, 26].

III. PARTITIONING AND LOCALISATION

ROI size is an important consideration in implementing the search algorithm described in the previous section. Theoretically, the size must reasonably be large to enable ROI to contain sufficient information for precise PSF estimation. For simplicity, a square ROI of size $W = 2^n \times 2^n$, where n is an integer, is considered.
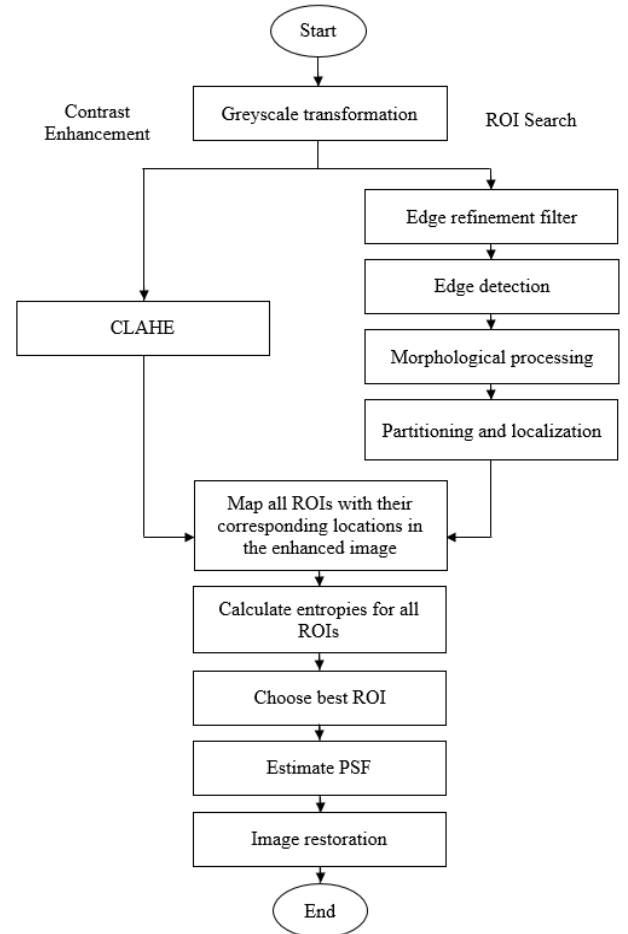

Figure 1. Overall procedure of the proposed method.

For example, the size of each block for a fixed square block of $N \times N$ is given as follows:

$$N = 2^{n-s}, \qquad (13)$$

where s is an integer above 0. The variable s controls the

size of each ROI block. The number of ROI block d that results from this partitioning is calculated as follows:

$$d = 2^{2s}. \tag{14}$$

For example, $d = 4$ and $N = 512$ for $n = 10$ and $s = 1$, respectively. Similarly, $d = 16$ and $N = 256$ for $n = 10$ and $s = 2$. For a given N, s and d values, partitioning and localisation are performed to retrieve all possible locations of ROIs. In this case, an ROI is characterised by pixels with high gradient values with minimum amount of noise.
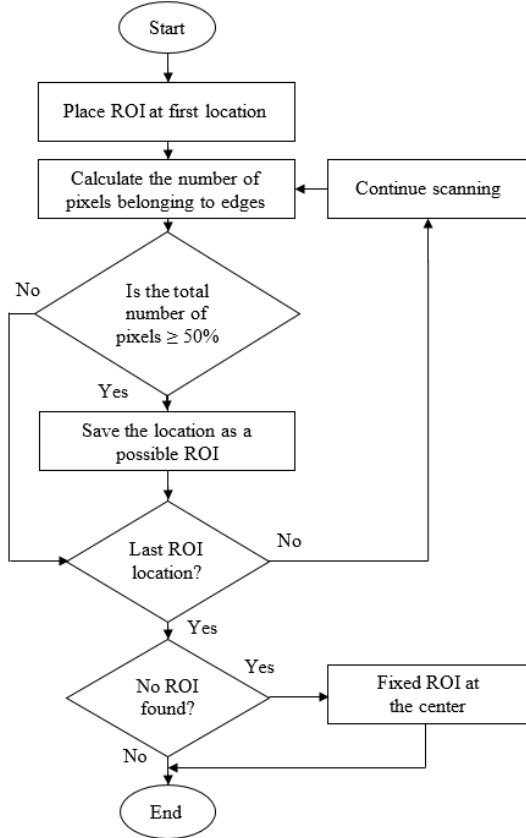

Figure 2. Flowchart summarising the algorithm for ROI search based on edge-driven partitioning and localisation.

Fig. 2 summarises all important procedures in retrieving all possible ROI candidates. The specific procedures include the following important steps. Firstly, W is placed at the top left-hand corner of the image. Secondly, W is moved across the image, one row at a time, from top to bottom, until the entire image has been scanned. This process is similar to raster scanning in digital devices. Hence, this strategy provides more candidate solutions than merely searching for non-overlapping blocks. At each location, the number of pixels belonging to the edges are counted in W. In this case, the number must be at least 50% of the total number of pixels to consider W the ROI's candidate. This threshold limit is established heuristically. Lastly, each ROI that satisfies this requirement is stored for further processing. In the event that no W satisfies this requirement, ROI is simply mapped to the centre of the image, which is also a default ROI location.

IV. TEST IMAGES

Three data sets are used to evaluate the performance of the proposed technique: Data set I, Data set II and Data set

III. Data set I is used for edge evaluation and Data sets II and III are reserved for BID restoration. Data set I consists of 15 selected RGB images together with their ground truth contours. They are obtained from the Berkeley Segmentation Dataset (BSDS500) [27]. The size of each image is 482×321 pixels. All images in this data set are blurred using 8 different PSF kernels for a total of 120 blurry images. All PSF kernels in the current study are obtained from the literature [1].

Data set II consists of 10 greyscale images obtained from [11]. Overall, this data set has 10 different test images, which are referred as IMG1, IMG2 and so on. Each image is convolved using 4 different PSF kernels, thereby resulting in 40 blurred images. Data set III contains one actual blurred image. This image was captured by the authors with a slightly out-of-focus camera and serves as an indicator of the effectiveness of the proposed solution.

V. QUALITY INDICES

Five quality indices are used to quantitatively evaluate the performance of the proposed algorithm: (i) Pratt's figure of merit (PFoM), (ii) two-fold consensus ground truth (TCGT), (iii) peak signal-to-noise ratio (PSNR), (iv) kernel similarity (KS) index and (v) error ratio (ER). In this case, PFoM and TCGT are used to assess the quality of the edges detected by the proposed method. PFoM is formulated as follows [28]:

$$PFoM = \frac{1}{\max(N_I, N_D)} \sum_{i=1}^{N_D} \frac{1}{1 + \beta d_i^2}, \tag{15}$$

where N_I and N_D are the number of ideal and detected edge pixels, respectively; β denotes a scaling constant used to penalise displaced edges and d_i is the Euclidian distance from an estimated edge point to the nearest ideal or ground truth edge pixel. The separation distance d_i plays a vital role in the evaluation of PFoM. Edge detection is considered good if the value of PFoM approximates 1 and poor when this value tends to 0.

The second quality index is TCGT proposed by Lopez–Molina et al. [29]. TCGT is a quantitative error measure for boundary detection based on the strong and weak consensus of a set of binary images. TCGT can be expressed as follows:

$$TCGT(E, S) = \frac{2 \cdot R_T(E, S) \cdot N_T(E, S)}{R_T(E, S) + N_T(E, S)}, \tag{16}$$

where E is a candidate image, S is a ground truth boundary image and R_T and N_T are the amount of compulsory information and spurious detections, respectively. The TCGT output of 0 and 1 represents the optimal and worst possible outcomes, respectively.

The remaining three indices are used to evaluate the performance of the proposed ROI search scheme. In this case, PSNR is calculated as follows [30]:

$$PSNR = 10\log_{10}\left[\frac{R^2}{MSE}\right] \tag{17}$$

and the mean squared error is given as follows:

$$MSE = \frac{\sum_{m=0}^{M-1}\sum_{n=0}^{N-1}\left(I_1(m,n) - I_2(m,n)\right)^2}{M \times N}, \quad (18)$$

where R, $I_1(m,n)$ and $I_2(m,n)$ are the maximum fluctuation in the input, actual and noisy images, respectively. Evidently, the higher the PSNR in this case, the more accurate the restoration. The KS index is used to compare the estimated kernel with the ground truth kernel. This index is formulated as follows [11]:

$$\rho(K,\hat{K},\gamma) = \frac{\sum_{\tau} K(\tau) \cdot \hat{K}(\tau + \gamma)}{\|K\| \cdot \|\hat{K}\|}, \quad (19)$$

where $\rho(\cdot)$ is the normalised cross-correlation function, K and $\hat{K}$ are the ground truth and estimated kernel, respectively, γ is the distances or error between the ideal and calculated kernels, τ represents the image coordinates and $\|\cdot\|$ indicates the Euclidean norm. Meanwhile, $K(\tau)$ and $\hat{K}(\tau)$ are 0 when τ is out of the kernel range. The larger the KS index, the more accurate the kernel estimation. Lastly, the fifth ER index measures the accuracy of the deconvolution process, and is defined as follows [1]:

$$ER = \frac{(x_{out} - x_{gt})}{(x_{kgt} - x_{gt})}, \quad (20)$$

where x_{out}, x_{gt} and x_{kgt} are the restored image using the estimated kernel, ground truth image and restored image using the ground truth kernel, respectively. An ER of 1 is ideal, although high ratios indicate results with limited accuracy.

VI. RESULTS AND DISCUSSION

The edge results from Data set I are compared with He et al. [16], Trujillo–Pino et al. [29], Jia et al. [30] and other popular filters. Meanwhile, the results from Data sets II and III are compared with the images restored using the ROI location determined using the default method and state-of-the-art methods published of Hu and Yang [11], Li et al. [12] and Ma et al. [13]. All experiments are performed using MATLAB® software package in a quad-core desktop computer.

A. ROI Size

Prior to restoration, a few experiments are initially performed to investigate the variation on entropy with ROI size. Three ROI sizes are considered, corresponding to $s = 1$, 2 and 3. Fig. 3 shows the results, which compare the proposed and existing methods.

As shown in Fig. 3, the entropies calculated from ROIs retrieved using the proposed method are consistently the highest, thereby indicating that they contain the most amount of information. This figure also shows that the proposed method resulted in nearly uniform entropy, averaging at 6.64 for all s. By contrast, ROI fixed at the centre of the image or the default method produced a maximum entropy of 7.0. However, this value decreased

significantly to 5.8 when s is increased from 1 to 3. Similarly, the entropy calculated by Hu and Yang [11] decreased from 7.2 to 6.5 with increasing s. No significant difference was observed between the results of Li et al. [12] and Ma et al. [13]. This outcome was obtained despite the entropies calculated by these methods are slightly higher than those computed by Hu and Yang [11]. Nevertheless, these values remain less than those of the proposed approach.
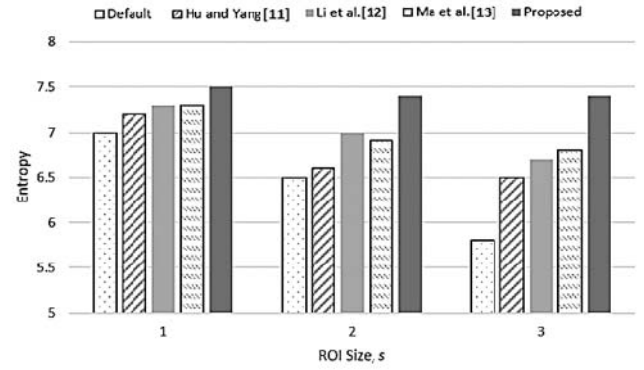

Figure 3. Evaluation of the ROI size in terms of entropy measure, comparing proposed and established methods.

Evidently, these results show that the amount of information produced by ROIs retrieved by default and Hu and Yang [11] are size-dependent. That is, the larger the ROI size (or smaller s), the higher the information. By contrast, the proposed method produces entropy, which is nearly independent of s, thereby indirectly indicating that ROI it retrieves is nearly optimal. This trend suggests that the ROI size in the proposed approach does not significantly impact the accuracy of the PSF estimation and, ultimately, the image restoration. Nevertheless, ROI in the current study is fixed to 150 × 150 to enable comparison with recent techniques.

B. Gaussian Parameters

In the proposed edge refinement filter, two parameters are required in the design of the Gaussian filter: (i) cut-off frequency σ and (ii) filter size. Therefore, two simulation experiments are performed to study the effects of σ and filter size on edge quality. In the first experiment, the edge detection is performed by fixing the filter size to 3 × 3 whilst varying σ from 0.3 to 0.7 in three discrete steps. Examples of edge images obtained through this procedure are shown in Fig. 4. Accordingly, no significant changes in the edges are detected in response to different σ values (see Fig. 4). Visually, all images appear relatively the same. The reason is mainly due to the blurriness of the input images, thereby making the overall process in edge detection minimally sensitive to σ.

Meanwhile, the results on varying the filter size on edge detection accuracy are shown in Fig. 5. Six filter sizes are considered: 3 × 3, 5 × 5, 7 × 7, 9 × 9, 19 × 19 and 29 × 29. Different from σ, a strong relationship exists between filter size and edge detection. Generally, the smaller the filter size, the better segmentation. In this case, the 3 × 3, 5 × 5, 7

Figure 4. Selected edge detection results from Data set I using the proposed method, (a) original image, (b) blurred version of (a), (c) ground truth edges and (d–f) correspond to edge detection results produced with 3 × 3 filter size for various σ values, 0.3, 0.5 and 0.7, respectively.
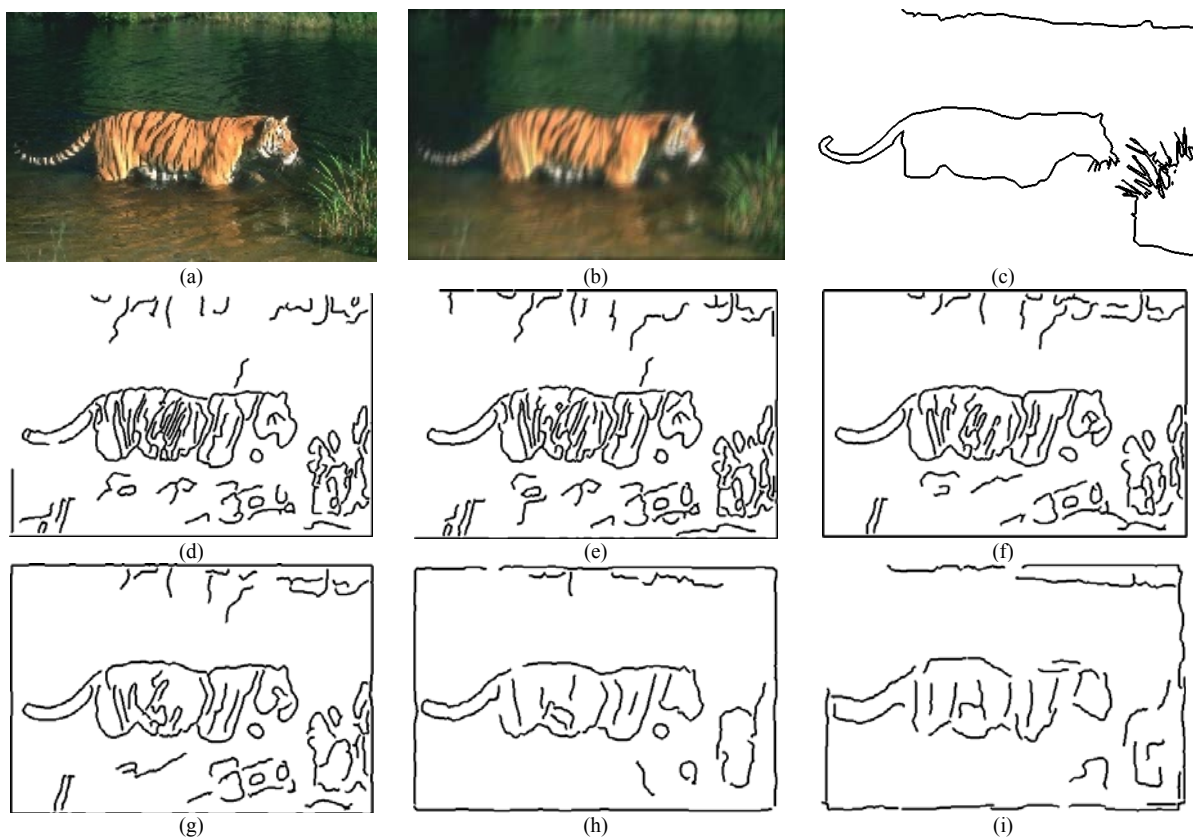

Figure 5. Selected edge detection results from Data set I using the proposed method, (a) original image, (b) blurred version of (a), (c) ground truth edges and (d–i) correspond to edge detection results produced with σ = 0.3 for various filter sizes, 3 × 3, 5 × 5, 7 × 7, 9 × 9, 19 × 19 and 29 × 29, respectively.

× 7 or 9 × 9 filter sizes yielded considerably more complete edges than larger size kernels, as shown in Figs. 5(d–g). Visually, many edges are missing when the 19 × 19 or 29 × 29 size kernels are used, thereby resulting in poorly segmented results (Figs. 5(h–i)). Therefore, the Gaussian filter in this application is designed with σ and the filter size set to 0.3 and 3 × 3. This filter is used in all deblurring experiments in this study.

C. Edge Evaluation

The objective and subjective assessments are used to evaluate the performance of the proposed edge refinement filter. Subjective evaluation is implemented through the visual comparison of the results using the proposed method and the methods of Sobel, LoG, Canny, He et al. [16], Trujillo–Pino et al. [18] and Jia et al. [19]. Table 1 summarises the quantitative evaluation of these results in terms of the PFoM and TCGT values calculated from all blurred images in Data set I. Table 1 shows that the proposed algorithm generally performs considerably better than the other established methods in terms of PFoM. In this case, the proposed method resulted in the best PFoM, averaging at 0.157. The next best performer is the method of Trujillo–Pino et al. [18] with an average PFoM of 0.147, followed by 0.151 in Jia et al. [19], 0.152 in He et al. [16],

TABLE I. AVERAGE EDGE EVALUATION RESULTS COMPARING THE PROPOSED AND ESTABLISHED METHODS.

Quality Indices	Kernel Groups	Sobel	LoG	Canny	He et al. [16]	Trujillo-Pino et al. [18]	Jia et al. [19]	Proposed
PFoM	H1	0.110	0.130	0.140	0.140	0.142	0.176	0.185
	H2	0.105	0.112	0.134	0.165	0.153	0.152	0.166
	H3	0.130	0.138	0.143	0.161	0.161	0.162	0.171
	H4	0.076	0.107	0.119	0.137	0.135	0.132	0.137
	H5	0.114	0.122	0.137	0.154	0.162	0.160	0.169
	H6	0.110	0.113	0.116	0.138	0.138	0.140	0.141
	H7	0.096	0.105	0.117	0.141	0.141	0.142	0.142
	H8	0.090	0.091	0.114	0.143	0.142	0.140	0.144
TCGT	H1	0.776	0.711	0.337	0.282	0.279	0.279	0.277
	H2	0.803	0.657	0.352	0.305	0.301	0.300	0.297
	H3	0.765	0.669	0.297	0.260	0.262	0.258	0.239
	H4	0.814	0.791	0.378	0.357	0.331	0.330	0.312
	H5	0.777	0.724	0.304	0.279	0.265	0.256	0.248
	H6	0.830	0.799	0.387	0.335	0.335	0.332	0.330
	H7	0.792	0.683	0.379	0.330	0.324	0.311	0.303
	H8	0.825	0.810	0.389	0.324	0.319	0.305	0.291

0.128 in Canny, 0.115 in LoG and 0.105 in Sobel. Although the PFoM values produced by the algorithms of Trujillo–Pino et al. [18], Jia et al. [19] and He et al. [16] are also competitive, the PFOM values calculated from all image kernels through the proposed solution are consistently higher than the PFoM values produced by these state-of-the-art techniques. An exception to this trend is the H4 and H7 kernels, in which the proposed method resulted in the same PFoM value compared with that of He et al. [16] and Jia et al. [19], respectively. Similarly, the proposed method produced the smallest value on the TCGT scale, thereby making it the best performer. On this scale, the proposed scheme yielded values with an average of 0.287, followed by 0.302 in Trujillo–Pino et al. [18], 0.296 in Jia et al. [19], 0.309 in He et al. [16], 0.353 in Canny, 0.731 in LoG and 0.798 in Sobel. Therefore, these results suggest that the improved edge refinement filter helps to locate and recover important edges in spite of the blurriness of the input images.

Fig. 6 shows three selected results and their ground truths, in which the Sobel operator resulted in the under thresholded image. The majority of the notable edges remained unsegmented, as depicted in Figs. 6(d)(i–iii). Similarly, the LoG method reconstructs the edges, but only a few contours are detected, as shown in Figs. 6(e)(i–iii). A close inspection of this figure reveals that the strongest contours are detected, but the weak and least significant edges remained unaccounted for. The difficulty in detecting minor edges is mainly due to the blurry nature of the input images.

By contrast, Canny's method appears to perform slightly better than those of Sobel and LoG. However, the majority of the images appear noisy, which is an extremely common drawback of this algorithm. Many significant edges are corrupted with unwanted pixels or noise, as shown in Figs. 6(f)(i–iii). Meanwhile, the method proposed by He et al. [16] yields comparable results. This method segments the majority of the edges, but some significant edges remain missing. Moreover, some 'false' edges are detected along with the accurate edges, as shown in Figs. 6(g)(i–iii). Figs. 6(h)(i–iii) and 6(i)(i–iii) show the edges produced by the algorithms proposed by Trujillo–Pino et al. [18] and Jia et al. [19], respectively. Although the majority of the important features in the three sample images appear clearly, the binarised images are filled with noise and interference. The deblurring would be less effective if such edge results

are used to determine the ROI. As shown in Fig. 6 and compared with the results of the existing techniques, the proposed method is more resistant to blur because the algorithm produces more complete edge information. Nearly every important edges are detected, and the images appear relatively clean with minimal amount of noise, as shown in Figs. 6(j)(i–iii).

D. ROI Evaluation – Data set II

This section uses the images in Data set II to summarise the performance of the proposed and established methods in terms of PSNR, KS Index and ER. For comparison, the average PSNR, KS index and ER values are calculated and plotted in Figs.7, 8 and 9 respectively.

In terms of PSNR, the results in Fig. 7(a) indicate a difference of 9.94 % between the highest and lowest PSNRs for all methods evaluated. Generally, the proposed method outperforms the other techniques, with the highest PSNR of 29.21 dB obtained from IMG5. The other methods produced moderate PSNRs, with an average of 28.26 dB. Although the difference in dB is relatively small, the slight decrease in PSNR causes a significant increase in the ringing artefacts of the restored outputs. Similarly, the proposed method produces substantially superior results for IMG1, IMG3, IMG4, and IMG5, with PSNR having an average of 27.80 dB.

A close examination of IMG5 reveals that no significant difference exists in terms of the PSNR values produced by the proposed method and those calculated from the default method and that of Hu and Yang [11]. This finding is due to the fact that this image is texturally less complicated, comprising mostly smooth or uniform regions. Thus, only a few ROI candidates are retrieved from this image compared with those from other substantially complex images. Moreover, the majority of ROIs retrieved are located near the centre of the image. They are also located near the default ROI and that calculated by Hu and Yang [11]. As expected, the quality of restored outputs is relatively the same as that in the PSNR results. Meanwhile, Fig. 7(b) compares the performance of each method in terms of the KS index. The proposed scheme is consistently more competitive than the other methods for all images tested. In this case, the best performance is obtained from IMG3, in which the proposed method produces the highest KS score,
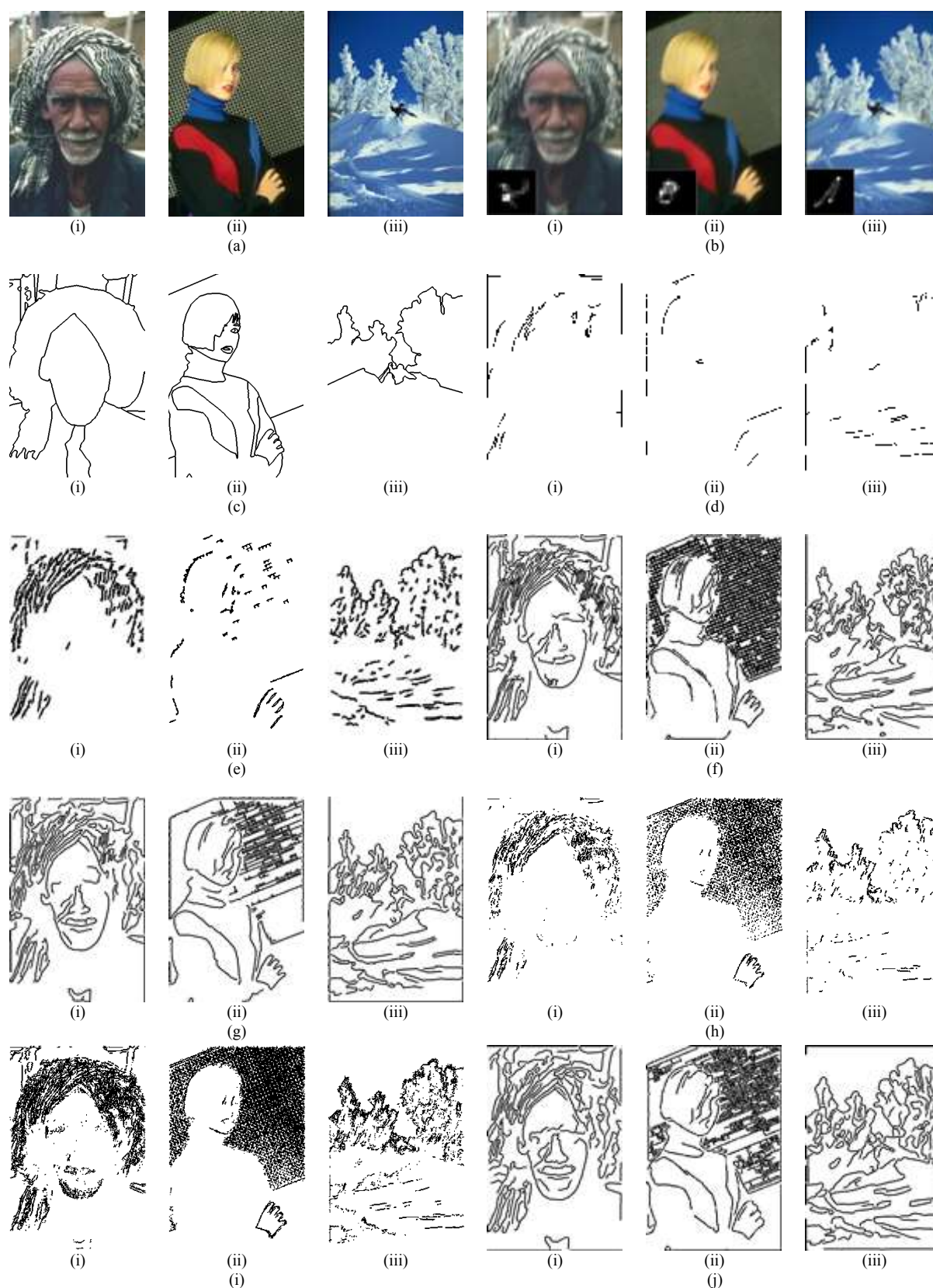
Figure 6. Edge detection of three selected images from Data set I. (a)(i–iii) test images, (b)(i–iii) blurred version of (a) together with the kernels responsible for blurring, (c)(i–iii) ground truth edges, and (d)(i–iii), (e)(i–iii), (f)(i–iii), (g)(i–iii), (h)(i–iii), (i)(i–iii) and (j)(i–iii) are edge results produced by Sobel, LoG, Canny, He et al. [16], Trujillo–Pino et al. [18], Jia et al. [19] and the proposed methods, respectively.

with an average of 0.89 compared with 0.87 in Li et al. [12], 0.87 in the default, 0.86 in Hu and Yang [11] and 0.85 in Ma et al. [13]. By contrast, the results from IMG2 and IMG6 are the worst for all the methods investigated. Hence, the proposed method is considered the best. The reason for the slight decrease in the performance is the fact that both images contain many repeated but identical patterns. For

example, IMG2 features a zebra with stripes that are uniquely identical, whilst IMG6 contains many small tree branches that appear similar. The presence of many similar patterns in these images causes some difficulties in selecting an accurate ROI on the basis of entropy measurement feedback.

Fig. 7(c) illustrates the performance of the proposed method in terms of ER. This figure clearly shows that the proposed scheme yields the lowest ER scores for all images, with an average of 1.09 compared with 1.11 in the default, 1.12 in Hu and Yang [11], 1.12 in Li et al. [12] and 1.13 in Ma et al. [13]. The worst performance is from IMG6 owing to the same reason as previously discussed. Nevertheless, the proposed approach is considered the best, thereby indicating its competitive precision compared with the other methods.
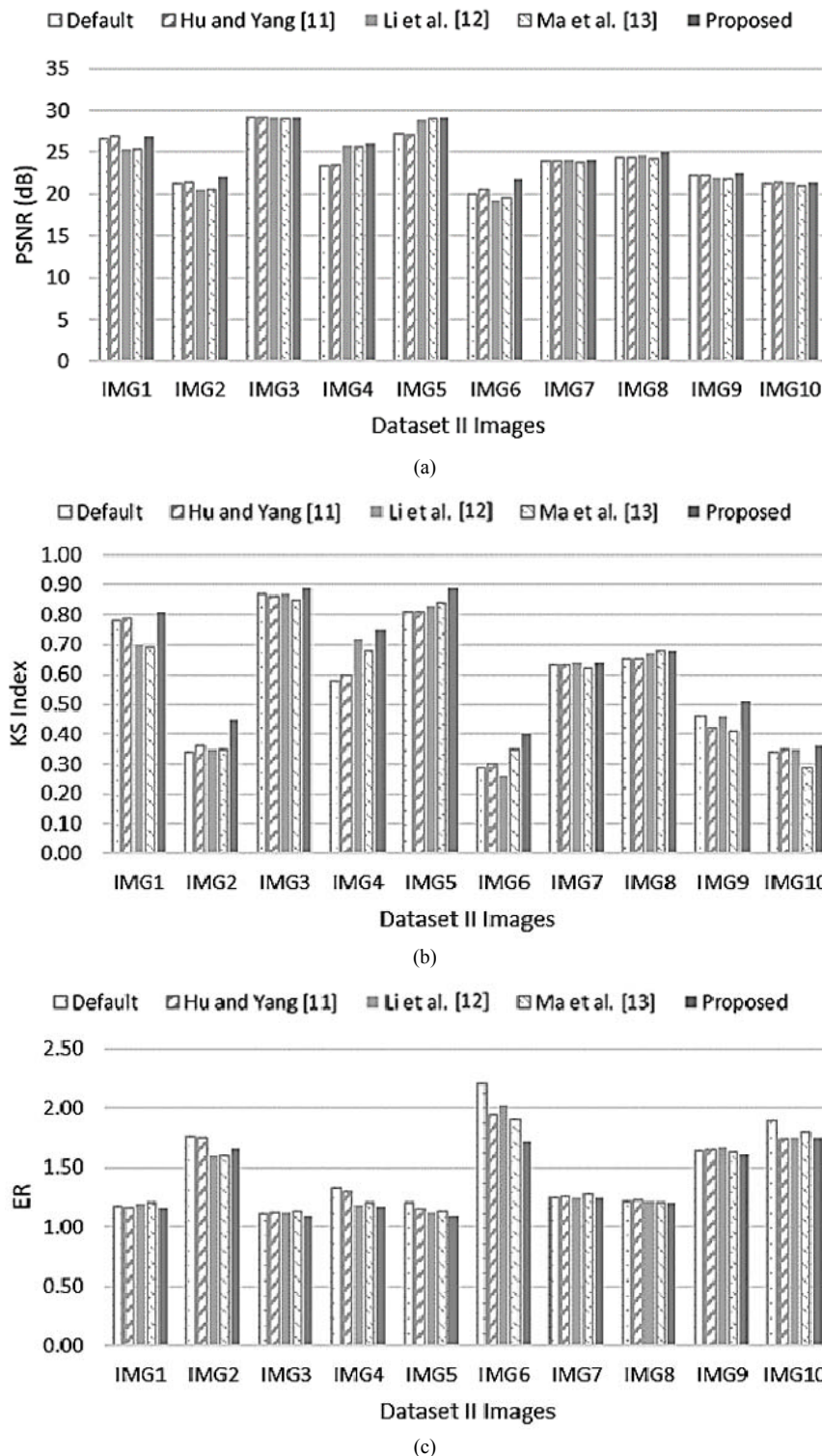

(a)

(b)

(c)

Figure 7. Performance of the proposed method in terms of (a) PSNR, (b) KS Index and (c) ER compared with the existing techniques.

By contrast, the ER values calculated from the default ROI are consistently the lowest, as shown in IMG2, IMG6 and IMG10. This result suggests that this method is effective when the edges are concentrated at the centre of the image. However, the proposed technique constantly leads to a region containing dominant edges regardless of their location in the image. Overall, the proposed method achieves superior accuracy and performance in terms of the PSNR, KS and ER measures. Further evidence is provided in Fig. 8, which shows the quality of selected deblurring results along with the calculated PSF kernels.
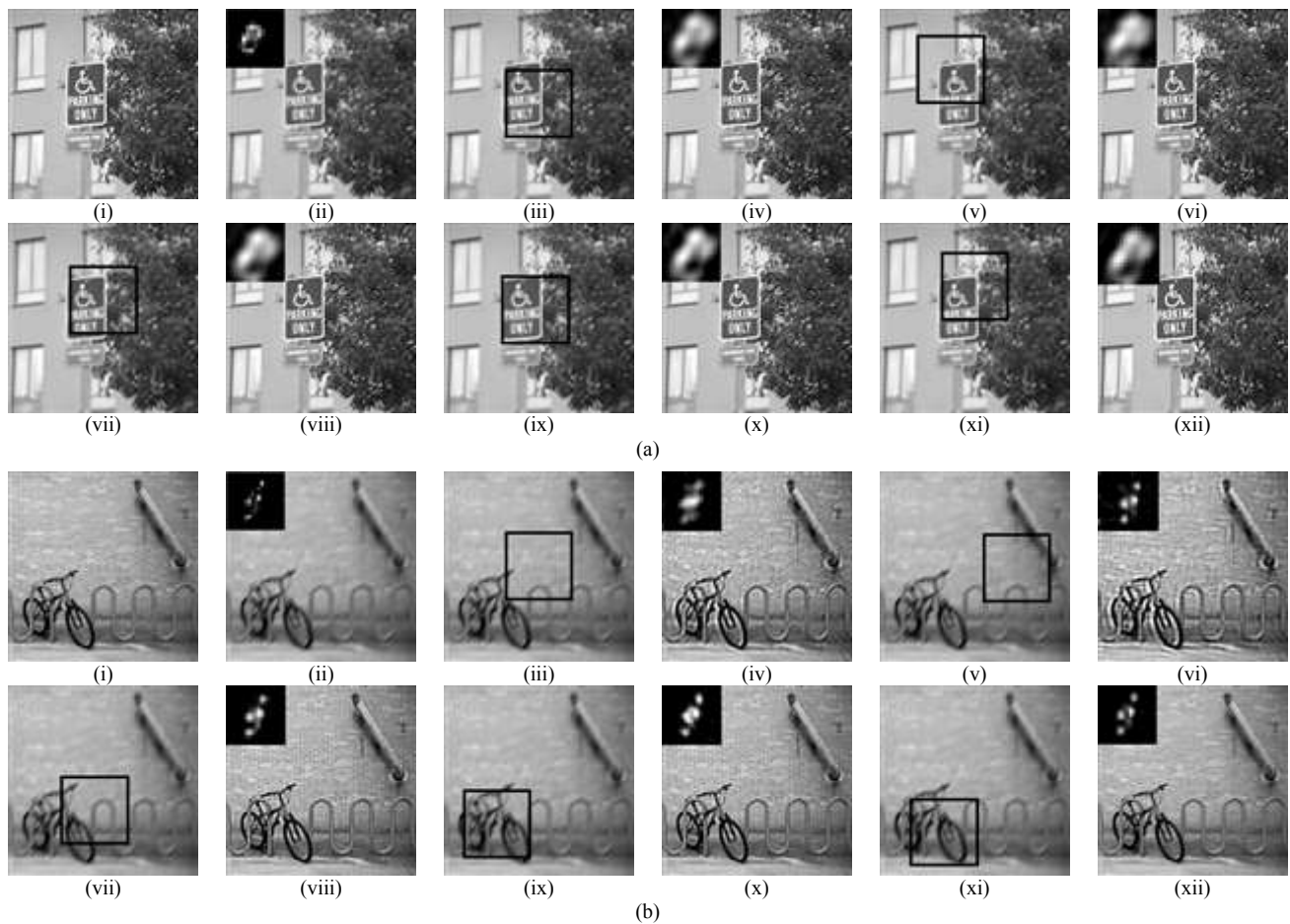
Figure 8. (a–b) Image restoration results of two selected blurred images from Data set II. (i–ii) Ground truths and the corresponding blurred versions together with the actual blurring kernels, (iii–iv) restored images using the default ROI locations together with estimated PSF kernels, (v–vi) restored images using ROIs estimated by Hu and Yang [11] together with the estimated PSF kernels, (vii–viii) restored images using ROIs estimated by Ma et al. [13] together with the estimated PSF kernels, (ix–x) restored image using ROIs estimated by Li et al. [12] together with estimated PSF kernels, and (xi–xii) restored images using ROIs estimated by the proposed method together with estimated PSF kernels.

E. ROI Evaluation – Data set III

To complete the investigation, the performance of the proposed scheme is also evaluated using one actual blurred image in Data set III. The results are presented in Fig. 9. A close examination of Fig. 9(a)(ii) revealed no significant improvement in the image quality as a result of applying the default ROI. This effect can clearly be visualised in the close-up view in Fig. 9(a)(iii). In this case, numbers '2' and '3' appear relatively blurry.

A slight improvement can be observed using the methods of Hu and Yang [11], Li et al. [12] and Ma et al. [13], as shown in Figs. 9(b)(ii), 9(c)(ii) and 9(d)(iii), respectively. Although these methods have resulted in substantially sharp images, the results contain ringing artefacts, as shown in Figs. 9(b–d)(iii). Evidently, the numbers '2' and '3' appear distorted owing to the presence of ringing artefacts. Meanwhile, Fig. 9(e)(ii) shows the restored result using ROI retrieved through a proposed algorithm. Visually, this image appears considerably sharper with less ringing artefact than the close-up view in Fig. 9(e)(iii). Therefore, this result indicates a definite superiority of the proposed approach to existing methods. It also indirectly proves that the ROI retrieved by the proposed scheme is nearly optimal, thereby leading to substantially precise PSF estimation and accurate restoration.

VII. CONCLUSION

Edges are increasingly utilised to determine the ROI location for image deblurring based on BID procedures. Recent studies have shown that regions containing strong edges tend to produce superior deblurring results. The conventional gradient-based approaches have high false positive because the majority of these methods favour salient or short edges. Therefore, selecting a small region with meaningful edges is preferred instead of an entire image for estimating the PSF. The current study presents a new direct method for retrieving a near-optimal ROI. The proposed method is a combination of an improved edge refinement filter and entropy feedback measurement. The performance of the proposed method is investigated qualitatively and quantitatively using three data sets comprising simulated and actual blurred images. Given the experimental results, the proposed solution generates substantially complete edges and demonstrates good performance on PFoM and TCGT scales. Similarly, the proposed ROI retrieval scheme resulted in considerably accurate restoration in terms of the PSNR, KS and ER measures.
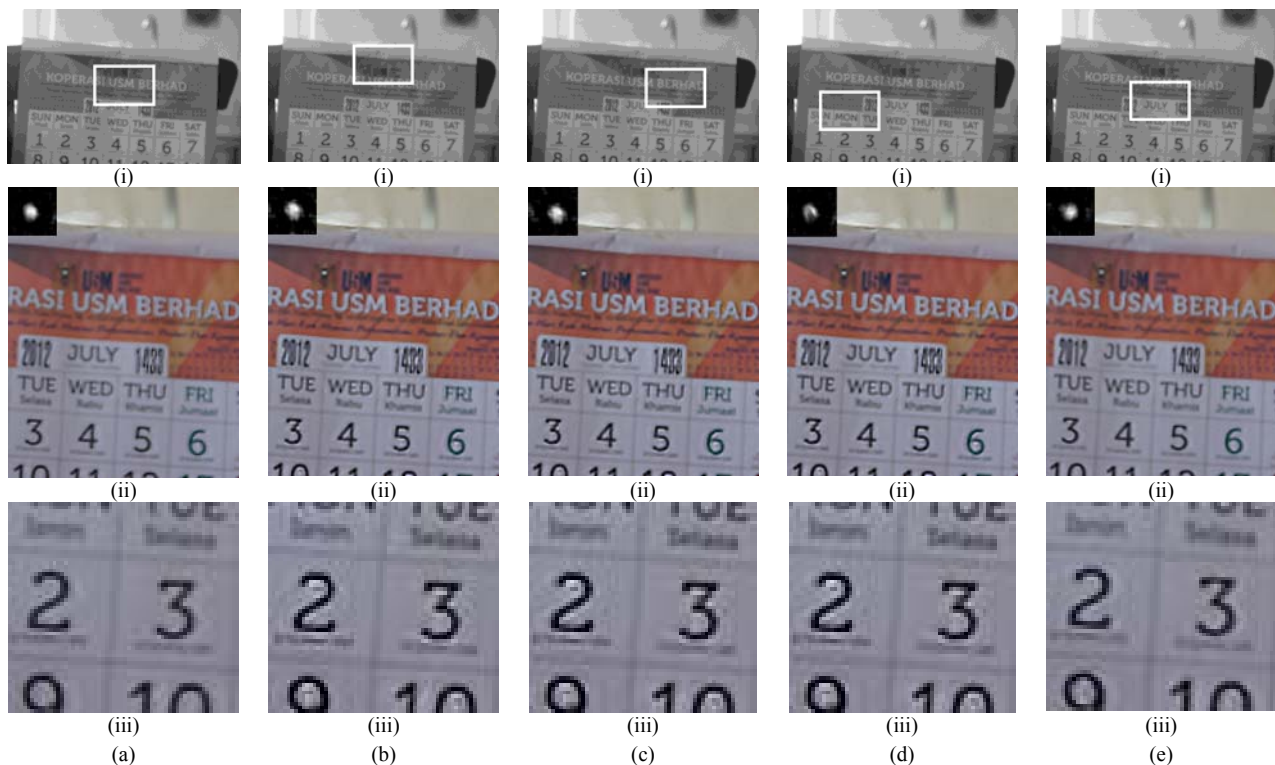
Figure 9. Image restoration of the first test image from Data set III comparing the proposed and established methods. (i) blurred images, (ii) their restored counterparts and (iii) close-up view of each restored image. In this case, (a), (b), (c), (d) and (e) correspond to deblurring results produced by default, Hu and Yang [11], Ma et al. [13], (d) Li et al. [12] and (e) proposed methods, respectively. Small square blocks in (i) show ROIs retrieved by each method, and the estimated kernel is included at the top-left hand corner in each restored output.

REFERENCES

[1] A. Levin, Y. Weiss, F. Durand, and W.T. Freema, "Understanding blind deconvolution algorithms", IEEE Transactions on Pattern Analysis and Machine Intelligence, vol. 33, no. 12, pp. 2354-2367, 2011. doi: 10.1109/TPAMI.2011.148

[2] C.J. Schuler, M. Hirsch, S. Harmeling, and B. Schölkopf, "Learning to deblur", IEEE Transactions on Pattern Analysis and Machine Intelligence, vol. 38, no. 7, pp. 1439-1451, 2015. doi: 10.1109/TPAMI.2015.2481418

[3] J. Wen, J. Wu, F. Zhang, R. Wei, and X.L. Xing, "Improved TV for blind deblurring with split Bregman iteration", The Imaging Science Journal, vol. 64, no. 3, pp. 160-165, 2016. doi: 10.1080/13682199.2016.1157955

[4] J. Pan, R. Liu, Z. Su, and X. Gu, "Kernel estimation from salient structure for robust motion deblurring", Signal Processing: Image Communication, vol. 38, no. 9, pp. 1156-1170, 2013. doi: 10.1016/j.image.2013.05.001

[5] R.R. Choudhary, A. Jangid, and G. Meena, "A novel approach for edge detection for blurry images by using digital image processing", in 2017 IEEE International Conference on Current Trends in Computer, Electrical, Electronics and Communication (CTCEEC), 2017, pp. 1029-1034. doi: 10.1109/CTCEEC.2017.8455081

[6] Z. Ying, C. Cai, Z. Liu, and Y. Ming, "A high precision edge detection method for the blurred image in motion measurement", in 10th International Symposium on Precision Engineering, Measurements and Instrumentation, 2019, pp. 110532. doi: 10.1117/12.2511940

[7] Y. Li, L. Xu, H. Jin, and J. Zou, "Localizing edges for estimating point spread function by removing outlier points", Journal of Modern Optics, vol. 63, no. 3, pp. 245-251, 2016. doi: 10.1080/09500340.2015.1074738

[8] W. Li, X. Cui, V.H. Nguyen, T.D. Do, I. Park, and H. Kim, "Blind image deconvolution based on robust stable edge prediction", in 2016 IEEE-EMBS International Conference on Biomedical and Health Informatics (BHI), 2016, pp. 66-69. doi: 10.1109/BHI.2016.7455836

[9] S. Cho and S. Lee, "Fast motion deblurring", ACM Transactions on graphics (TOG), vol. 28, no. 5, pp. 145, 2009. doi: 10.1145/1618452.1618491

[10] J. Pan, R. Liu, Z. Su, and X. Gu, "Kernel estimation from salient structure for robust motion deblurring", Signal Processing: Image Communication, vol. 28, no. 9, pp. 1156-1170, 2013. doi: 10.1016/j.image.2013.05.001

[11] Z. Hu, and M.H. Yang, "Learning good regions to deblur images", International Journal of Computer Vision, vol. 115, no. 3, pp.345-362, 2015. doi: 10.1007/s11263-015-0821-1

[12] L. Li, H. Yan, Z. Fan, H. Zheng, C. Gao, and N. Sang, "Selecting good regions to deblur via relative total variation", in 10th International Symposium on Multispectral Image Processing and Pattern Recognition, 2018, pp. 106090. doi: 10.1117/12.2284374

[13] C. Ma, J. Zhang, S. Xu, W. Meng, R. Xi, G.H. Kumar, and X. Zhang, "Accurate blind deblurring using salient patch-based prior for large-size images", Multimedia Tools and Applications, vol. 77, no. 21, pp. 28077-28100, 2018. doi: 10.1007/s11042-018-6009-2

[14] J. Pan, D. Sun, H. Pfister, and M.H. Yang, "Blind image deblurring using dark channel prior", in 2016 IEEE International Conference on Computer Vision and Pattern Recognition, 2016, pp. 1628-1636. doi: 10.1109/CVPR.2016.180

[15] J. Kotera, F. Šroubek, and D. Milanfar, "Blind deconvolution using alternating maximum a posteriori estimation with heavy-tailed priors", in International Conference on Computer Analysis of Images and Patterns, 2013, pp. 59-66. doi: 10.1007/978-3-642-40246-3_8

[16] K. He, J. Sun, and X. Tang, "Guided image filtering", IEEE Transactions on Pattern Analysis and Machine Intelligence, vol. 35, no. 6, pp. 1397-1409, 2012. doi: 10.1109/TPAMI.2012.213

[17] C. Tomasi, and R. Manduchi, "Bilateral filtering for gray and color images", in 1998 IEEE International Conference on Computer Vision, 1998, pp. 2. doi: 10.1109/ICCV.1998.710815

[18] A. Trujillo-Pino, K. Krissian, M. Alemán-Flores, and D. Santana-Cedrés, "Accurate subpixel edge location based on partial area effect", Image and Vision Computing, vol. 31, no. 1, pp.72-90, 2013. doi: 10.1016/j.imavis.2012.10.005

[19] X. Jia, H. Huang, Y. Sun, J. Yuan, and D.M. Powers, "A novel edge detection approach using a fusion model," Multimedia Tools and Applications, vo. 75, no. 2, pp.1099-1133, 2016. doi: 10.1007/s11042-014-2359-6

[20] T. Hasti, R. Tibshirani, J. Friedman, and J. Franklin, "The elements of statistical learning: data mining, inference and prediction", The Mathematical Intelligencer, vol. 27, no. 2, pp. 83-85, 2005. doi: 10.1007/BF02985802

[21] K. Dabov, A. Foi, and K. Egiazarian, "Video denoising by sparse 3D transform-domain collaborative filtering", in 15th IEEE European Signal Processing Conference, 2007, pp. 145-149. doi: 10.1109/TIP.2007.901238

[22] A. Makandar, and B. Halalli, "Image enhancement techniques using high pass and low pass filters", International Journal of Computer and

Applications, vol. 109, no. 14, pp. 12-15, 2015. doi: 10.5120/19256-0999

[23] W. Dong, S. Xiao, and Y. Li, "Hyperspectral sharpening based on guided filter and Gaussian filter", Journal of Visual Communication and Image Representation, vol. 53, pp. 171-179, 2018. doi: 10.1016/j.jvcir.2018.03.014

[24] B.S. Min, D.K. Lim, S.J. Kim, and J.H. Lee, "A novel method of determining parameters of CLAHE based on image entropy", International Journal of Software Engineering and its Applications, vol. 7, no. 5, pp. 113-120, 2013. doi: 10.14257/ijseia.2013.7.5.11

[25] A. Lesne, "Shannon entropy: a rigorous notion at the crossroads between probability, information theory, dynamical systems and statistical physics", Mathematical Structure in Computer Science, vol. 24, no. 3, pp. 1-63, 2014. doi:10.1017/S0960129512000783

[26] X. Zhou, J. Mateos, F. Zhou, R. Molina, and A.K. Katsaggelos, "Variational Dirichlet blur kernel estimation", IEEE Transactions on Image Processing, vol. 24. No. 12, pp. 5127-5139, 2015. doi: 10.1109/TIP.2015.2478407

[27] P. Arbelaez, M. Maire, C. Fowlkes, and J. Malik, "Contour detection and hierarchical image segmentation", IEEE Transaction of Pattern Analysis and Machine Intelligence, vol. 33, no. 5) pp. 898-916, 2010. doi: 10.1109/TPAMI.2010.161

[28] R. Varatharajan, K. Vasanth, M. Gunasekaran, M. Priyan, and X.Z. Gao, "An adaptive decision based kriging interpolation algorithm for the removal of high density salt and pepper noise in images", Computer & Electrical Engineering, vol. 70, pp. 447-461, 2018. doi: 10.1016/j.compeleceng.2017.05.035

[29] C. Lopez-Molina, B. De Baets, H. Bustince, "Twofold consensus for boundary detection ground truth", Knowledge-Based Systems, vol. 98, pp. 162-171, 2016. doi: 10.1016/j.knosys.2016.01.033

[30] K. Tutuncu, and B. Demirci, "Adaptive LSB steganography based on chaos theory and random distortion", Advances in Electrical and Computer Engineering, vol. 18, no. 3, pp.15-22, 2018. doi: 10.4316/AECE.2018.03003